Nucleopore-Inspired Polymer Hydrogels for

2 Selective Biomolecular Transport

- 3 Yun Jung Yang,[†] Danielle J. Mai,[†] Thomas J. Dursch, and Bradley D. Olsen*
- 4 †Y.J.Y. and D.J.M. contributed equally to this work
- 5 Department of Chemical Engineering, Massachusetts Institute of Technology, Cambridge, MA,
- 6 02139, United States

8

7 KEYWORDS: bioinspired materials, hydrogels, polymers, biomolecular transport

9 Biological systems routinely regulate biomolecular transport with remarkable specificity, low 10 energy input, and simple mechanisms. Here, the biophysical mechanisms of nuclear transport 11 inspire the development of Gels for Recognition And Selective Permeation (GRASP). GRASP 12 presents a new paradigm for specific transport and selective permeability, in which binding 13 interactions between a biomolecule and a hydrogel lead to faster penetration of the gel. A 14 molecular transport theory identifies key principles for selective transport: entropic repulsion of 15 non-interacting molecules and affinity-mediated diffusion of multi-receptor biomolecules through 16 a walking mechanism. The ability of interacting molecules to walk through hydrogels enables 17 enhanced permeability in polymer networks. To realize this theoretical prediction in a novel 18 material, GRASP is engineered from a polyethylene glycol network (entropic barrier) containing

- 1 antibody-binding oligopeptides (affinity domains). GRASP is synthesized using simultaneous
- 2 bioconjugation and polycondensation reactions. The elastic modulus, characteristic pore size,
- 3 biomolecular diffusivity, and selective permeability are measured in the resulting materials, which
- 4 are applied to regulate the transport of equally sized molecules by preferentially transporting a
- 5 monoclonal antibody from a polyclonal mixture. Overall, this work presents rationally designed,
- 6 nucleopore-inspired hydrogels that are capable of controlling biomolecular transport.

Introduction

- 8 Controlling transport in biological systems is critical to broad applications in biological toxin
- 9 removal, ^{1,2} blood sensing and diagnostics, ^{3,4} immune disorder treatments, ⁵ and therapeutic protein
- 10 purification.^{6, 7} Oftentimes, biomolecular cargo are present at low concentrations, share
- physicochemical properties with undesired biomolecules (size, hydrophobicity, and electrostatic
- 12 charge),⁸ and are required to move through crowded environments.⁹ Current approaches to
- 13 biomolecular detection,⁴ separation,⁷ and transport^{10, 11} utilize high-affinity interactions to
- 14 overcome these challenges; however, such systems require optimized changes in environmental
- 15 conditions to release biomolecular cargo. New materials for efficient biomolecular transport will
- subsequently improve protein sensing, purification, and delivery.
- 17 Nature has evolved systems that harmonize high- and low-affinity interactions to regulate
- molecular transport, resulting in remarkably selective biomolecular sorting and separations. ¹² One
- example is the nuclear envelope, which is a biopolymer membrane that critically regulates access
- 20 to a cell's precious genomic information. 13-16 During nuclear transport, biomolecular targets are
- 21 recognized by high-affinity interactions with nuclear transport receptor (NTR) proteins. 15 NTRs
- and their cargo are then selectively translocated through nuclear pore complexes (NPCs) that span

the nuclear envelope. In the NPC, phenylalanine-glycine-rich (FG) nucleoporin proteins form a space-filling protein matrix that prevents non-specific macromolecular transport. FG nucleoporins exhibit remarkable selectivity, rejecting the passage of 99.9% of all proteins. 14 NTRs and NTRcargo complexes overcome this entropic barrier by undergoing numerous, low-affinity interactions with FG domains in the protein matrix.¹⁷ Multivalent interactions can give rise to diffusion by walking through the matrix, 18-20 thereby enabling selective biomolecular transport. 21-24 The relationship between multivalent biomolecular walking and selective transport in a protein matrix can be elucidated using a molecular approach to transport theory. Modeling the diffusion of a solute through a hydrogel is a longstanding topic of interest, with classical transport theories focusing on the non-interactive barrier mechanisms of polymer or particulate networks.²⁵⁻²⁸ In these classical systems, interactions between solutes and the polymer network are either negligible^{25, 26} or strong and specific, leading to solute immobilization.^{27, 28} Recently, molecularbased transport theories have reconsidered the role of biomolecular binding kinetics on diffusivity in the context of intracellular mobility, ^{29, 30} lateral biomolecular transport at surfaces, ^{18, 19, 31} and self-diffusion in associative protein hydrogels. ^{20, 32, 33} Aspects of these binding-diffusion models can be applied to understand biomolecular solutes that interact with a polymeric hydrogel and to generate designs for selectively permeable hydrogels. The remarkable selective transport performance of the nuclear envelope has already inspired the development of novel materials that control biomolecular transport. Selective nucleoporin permeability has been replicated outside of the nuclear pore in protein hydrogels based on recombinant nucleoporins³⁴⁻³⁸ and artificially engineered, nucleoporin-inspired polypeptides.³⁹⁻⁴¹ Both classes of these nucleoporin-based recombinant proteins form associative hydrogels and incorporate numerous FG domains to facilitate the specific transport of NTRs and their cargo.

1

2

3

4

5

6

7

8

9

10

11

12

13

14

15

16

17

18

19

20

21

22

Molecular transport theory can identify design principles from nucleoporin-based proteins and apply mechanistic understanding to develop synthetic analogues to nucleoporins. This approach enables the development of materials with biochemical versatility to control the transport of new biomolecular targets, as well as improved mechanical properties by covalent crosslinking chemistries for hydrogel formation. Numerous approaches to synthetic, biocompatible hydrogels have been previously developed, including affinity hydrogels containing bioactive compounds⁴²or polypeptides. 47-51 These affinity hydrogels have been employed for biomolecular immobilization and controlled release in tissue engineering and drug delivery applications, predominantly based on selective adsorption-based mechanisms that differ substantially from those used to regulate protein permeability through the nuclear pore. Therefore, a synthetic mimic of this natural system could offer a substantially new material platform for biomolecular separation. In this work, molecular transport theory is applied to engineer nucleopore-inspired polymer hydrogels with selective biomolecular permeability. Nuclear transport mechanisms are incorporated into a protein binding-diffusion model to establish design criteria for polymeric materials that control selective protein transport. The theory identifies two key principles: (1) entropic repulsion of undesired biomolecules and (2) affinity-mediated permeability of target biomolecules. These principles guide the design and synthesis of Gels for Recognition And Selective Permeation (GRASP), which are applied to perform a model separation of monoclonal antibodies from a polyclonal antibody mixture.

1

2

3

4

5

6

7

8

9

10

11

12

13

14

15

16

17

18

19

Experimental Section (Materials and Methods)

1

2 Synthesis of Gels for Recognition And Selective Permeation (GRASP). GRASP consists of 3 antibody-binding oligopeptides embedded in a crosslinked poly(ethylene glycol) (PEG) hydrogel. 4 Oligopeptides were designed to have varying binding affinities to anti-c-Myc antibody (9E10). Five epitope sequences with varying dissociation constants⁵² were selected as binding domains, 5 6 which were flanked on both termini by glycine spacer residues to reduce steric hindrance and 7 cysteine residues for conjugation (sequences in Table 1). This study also included a negative 8 control peptide with the sequence CGGC. All custom peptides were synthesized commercially 9 (Genscript). Four-arm polyethylene glycol (PEG, 20 kDa) with maleimide end groups (Creative PEGWorks) was used for thiol-maleimide coupling⁵³ with di-cysteine peptides to form a 10 11 chemically crosslinked gel using A₂ + B₄ polycondensation chemistry. 12 For all experiments except small-angle neutron scattering (SANS), PEG was initially dissolved in 13 phosphate-buffered saline (PBS, pH 7.4) at 10% w/v. Separately, peptides were dissolved at 10% 14 w/v in PBS and reduced with a ten-fold molar excess of tris(2-carboxyethyl)phosphine (TCEP, 15 Sigma Aldrich). The reduced peptide solution was adjusted to pH 7.4 using sodium hydroxide and 16 equilibrated for 30 minutes at room temperature. The resulting PEG and peptide solutions were 17 combined to reach a 1:2 PEG-to-peptide molar ratio to maintain functional group stoichiometry 18 during gelation. Gels were cast in Teflon molds (rheology) or Eppendorf tubes (FRAP and 1D 19 transport assays) and allowed to set overnight. 20 Shear rheology. Small-amplitude oscillatory shear measurements were performed on an Anton 21 Paar MCR-301 rheometer operating with a disposable parallel plate geometry (10 mm diameter) 22 with roughened surfaces (sandpaper, Norton Abrasives) to avoid slipping. Frequency sweep

1 experiments were performed from 0.1 to 100 rad/s at 0.5% strain, which was confirmed to be in 2 the linear viscoelastic regime by strain sweep experiments (0.01–100% strain at 10 rad/s). All 3 measurements were taken at 25 °C using Peltier temperature control. Three samples were tested 4 for each gel, with reported elastic shear moduli representing the mean \pm one standard deviation. 5 Gel conversion was estimated using the elastic shear modulus and a modified gel point theory.⁵⁴ 6 Small-angle neutron scattering (SANS). SANS experiments were conducted at the Oak Ridge 7 National Laboratory Spallation Neutron Source (ORNL SNS) Extended Q-Range SANS 8 Diffractometer using a beam aperture of 8 mm. Phosphate-buffered deuterium oxide (137 mM 9 NaCl, 2.7 mM KCl, 10 mM Na₂HPO₄ and 1.8 mM KH₂PO₄ in D₂O) was prepared to facilitate neutron scattering contrast in SANS experiments. Buffer components were measured 10 11 gravimetrically to reach pD 7.4, and buffered D₂O was filtered using 0.2 µm Acrodisc syringe 12 filters (PALL Corporation). Gel precursor solutions were prepared as described above and cast 13 between quartz plates with a Teflon spacer (1 mm thickness, 13 mm inner diameter, 17 mm outer 14 diamater). The quartz sample sandwich was sealed overnight with silicone epoxy (Dow Corning) 15 prior to loading in a titanium cell. Scattering patterns were measured using two sample-to-detector 16 distances of 8 m and 2.5 m, using neutron wavelengths of 8 and 2.5 Å, respectively. These configurations covered a Q-range of 0.04–5.0 nm⁻¹. Scattering was performed at 25 °C. The raw 17 scattering intensity was reduced using the Mantid reduction package⁵⁵ and corrected for the 18 19 background from an empty sample cell and a sample cell containing buffered D₂O. Reduced SANS curves were fit using non-linear least-squares regression to a correlation length model. 56-58 20 21 Fluorescence recovery after photobleaching (FRAP). Prior to FRAP experiments, each GRASP 22 was equilibrated in a ten-fold volume of fluorescently labeled antibody solutions for at least 24

hours in the dark at 4 °C to ensure a homogeneous distribution throughout the gel. Antibody

1 solutions were used as received and contained either 3.3 µM fluorescein isothiocynate (FITC)-2 anti-c-Myc tag monoclonal antibody (9E10) (Thermo Fisher Scientific) or 3.3 µM FITC-IgG from 3 human serum (Sigma Aldrich) in PBS (pH 7.4) with 50% glycerol, 1% bovine serum albumin 4 (BSA), and 0.1% sodium azide. Each saturated GRASP was mounted on a glass coverslip for 5 imaging on a confocal laser scanning microscope (Zeiss LSM 710, W.M. Keck Microscopy 6 Facility) equipped with a water-immersion 40× objective lens (LD C-Plan Apochromat, NA 1.1). 7 A circular region of interest was photobleached using a 488 nm laser at full power, and 8 fluorescence recovery was monitored by scanning the region of interest at low laser power (24%) 9 every second for 1 minute after bleaching. A non-bleached gel region and background region were 10 also measured to normalize intensity as a function of time. Normalized intensity curves were 11 analyzed using non-linear least squares regression with a FRAP diffusion model.²⁹ 12 1D fluorescence transport assays. Rectangular borosilicate capillaries $(0.9 \times 0.9 \times 40 \text{ mm})$ Vitrocom) were loaded by piercing pre-made hydrogels.^{39, 40} For separate testing of anti-c-Myc 13 14 IgG or polyclonal IgG permeability (Figures 7a-b), commercial antibody–FITC solutions were 15 diluted to a final concentration of 1 µM and introduced to the exposed gel interface. Capillaries 16 were sealed with a wax mixture (equal parts Vaseline, lanolin, and paraffin) prior to imaging with 17 a Zeiss Axioplan fluorescence microscope equipped with an Axiocam 503 mono camera, FluoArc 18 control unit, and HBO 100 mercury plasma lamp. Images were acquired 5 minutes, 30 minutes, 19 and 60 minutes after the antibody solutions were added. 20 Two-color fluorescence microscopy was utilized to test anti-c-Myc IgG selectivity from a 21 polyclonal mixture. Immunoglobulin IgG from human serum (Sigma Aldrich) was fluorescently 22 tagged using Alexa Fluor® 594 NHS-ester (Thermo Fisher Scientific) according to manufacturer instructions. Excess fluorescent dye was removed after conjugation using an illustra NAPTM 10

column (GE Healthcare), and labeled IgG fractions were confirmed by SDS-PAGE. Any residual solvent or dyes were removed by dialysis against PBS (pH 8.3), and purified IgG–Alexa Fluor® conjugates were concentrated using an Amicon® Ultra-15 centrifugal filter (10 kDa molecular weight cutoff, MilliporeSigma). The final concentration and degree of labeling were determined by measuring absorbance at 280 and 590 nm. The degree of labeling was 3.9 dyes per molecule, which is within the generally accepted range of 2–5 dyes per protein required to minimize inactive and unlabeled antibodies. ⁵⁹ Polyclonal IgG–Alexa Fluor® 594 and commercial anti-c-Myc IgG–FITC (Thermo Fisher Scientific) were mixed to final concentrations of 1.65 μM each, and the resulting solution was used in the previously described 1D capillary geometry to test selective permeability of each GRASP. For each peptide sequence, three hydrogels were prepared and tested independently.

Results and Discussion

Binding–Diffusion Model for Selective Biomolecular Transport. The characteristics of polymer networks that control biomolecular transport are explored in the context of molecular transport theory by considering a continuum binding–diffusion model in the case of 1-dimensional transport through a membrane. The model enables the calculation of steady-state fluxes of specific and non-specific biomolecules through a polymer network. Molecular-scale characteristics of biomolecular solutes and polymer networks are derived from polymer physics and incorporated into the model to constrain relationships between continuum parameters. This approach identifies realistic parameter spaces for the design of selectively permeable polymer hydrogels. The model demonstrates a fundamentally new separation mechanism, in which permeation of a binding species is enhanced due to selective interactions and bound-state diffusive motion within the polymer network.

- 1 Governing equations and analytical solution for steady-state transport through a 1D membrane.
- 2 To model transport of a specifically interacting biomolecule through a polymer gel, consider a
- 3 polymer network with binding sites (S) that act as recognition domains for target biomolecular
- 4 solutes. Biomolecules exist as freely diffusing solutes (F) or in one of many bound states (B):

$$F + S \stackrel{\stackrel{k_{on}}{\longleftarrow}}{\longleftarrow} B \tag{1}$$

- 6 where k_{on} and k_{off} are the rates at which biomolecules bind to and unbind from the polymer network,
- 7 respectively (Figure 1a).

8

9

10

11

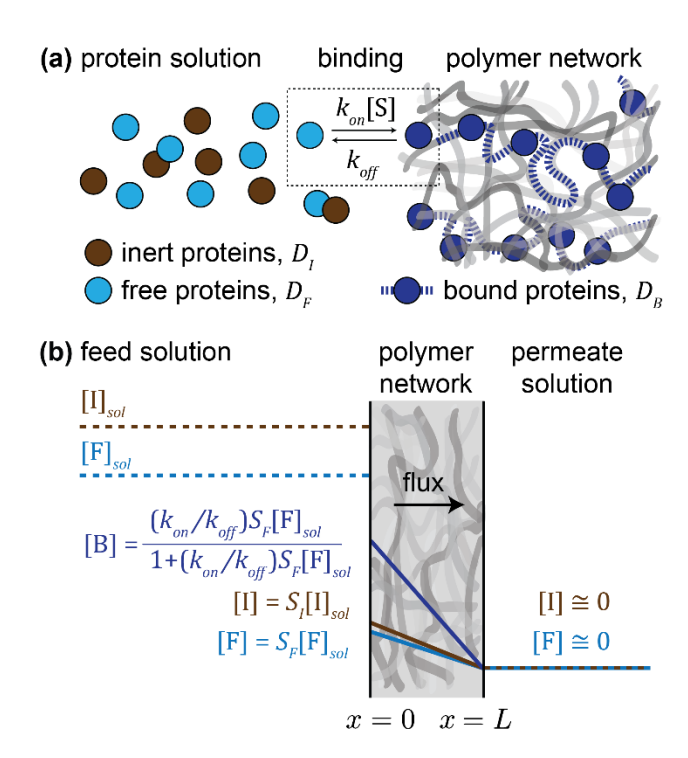


Figure 1. A binding–diffusion model (a) accounts for free and bound biomolecular diffusion in a polymer network and (b) is solved using boundary conditions for steady-state 1D transport in a polymer network of thickness L. Free solutes (F, aqua) and impurities (I, brown) partition according to solubilities S_F and S_I . Solutes bind (B, indigo) at the interface according to the

- 1 Langmuir adsorption model. A constant, zero-concentration boundary condition is assumed at the
- 2 second interface.

- 3 Binding reactions are reversible, and Fickian diffusion and binding are considered in the explicit
- 4 governing equations for transport, hereafter called the two-state model:

$$\frac{\partial[B]}{\partial t} = D_B \nabla^2[B] - k_{off}[B] + k_{on}[F][S]$$
 (2)

$$\frac{\partial[\mathbf{F}]}{\partial t} = D_F \nabla^2[\mathbf{F}] - k_{on}[\mathbf{F}][\mathbf{S}] + k_{off}[\mathbf{B}]$$
(3)

- where D_F is the diffusion coefficient of a free (unbound) biomolecule and D_B is the non-zero diffusion coefficient of biomolecules bound to the polymer network. Bound molecules may have nonzero diffusivities either if the network itself is dynamic, as is the case for biopolymer networks, or if the molecule is capable of walking across the network in a series of bound states, ^{18-20, 33} as discussed subsequently. In contrast, non-specific, inert biomolecules (I) only undergo Fickian diffusion. Similar binding–diffusion models that have been applied to study the impact of protein binding interactions on transport behavior assume that bound-state diffusivity is negligible on the time- and length-scales of interest;^{29, 33} however, it has been shown that a mobile bound state is necessary to fully capture diffusive dynamics in experiments and simulations.^{20, 32}
- The two-state model is solved analytically as a system of second-order differential equations by considering steady-state operation of a 1D polymer membrane of thickness L (**Figure 1b**), in the limit of dilute biomolecular solutes in comparison to polymer network recognition sites (constant [S]). In this limit, the rate of association is substituted with a pseudo-first-order rate constant (k_{on} [S] $\rightarrow k^*_{on}$). At the solute-rich interface, biomolecules bind non-cooperatively according to the Hill–Langmuir equation. Unbound solutes partition between solution and gel phases^{60, 61} according to solubilities S_F and S_I , which correspond to the partition coefficients for target and inert proteins,

- 1 respectively. A fixed, zero-concentration boundary condition is applied at the second interface to
- 2 model rapid removal of diffusing species from the membrane surface.
- 3 The flux of each species (J_i , i = B, F, or I) is directly calculated using the full analytical solution:

$$J_i(\infty, x) = -\frac{S_i[i]_{sol}}{L} \left[D_i \frac{\partial [i]^*}{\partial x^*} \right] \tag{4}$$

- 5 where $[i]^*$ and x^* are dimensionless concentration and length (details in the Supporting
- 6 Information, SI). The ratio of target protein flux to non-specific, inert protein flux is used to
- 7 identify parameter sets that give rise to selective transport. Selective transport occurs when
- 8 $(J_B+J_F)/J_I >> 1$. An expression for the flux ratio (details in SI) identifies key dimensionless
- 9 parameters involved in selective filtration:

$$\frac{\text{target flux}}{\text{inert flux}} = \frac{J_B + J_F}{J_I} = \delta \sigma^2 \left(\frac{1 + K_{eq}(\beta + \gamma)}{1 + K_{eq}\beta} \right)$$
 (5)

- where $\delta = D_F/D_I$ (diffusivity ratio), $\sigma = S_F/S_I$ (solubility ratio), $K_{eq} = k^*_{on}/k_{off}$ (equilibrium binding
- 12 constant), $\beta = [F]_{sol}/[S]$ (ratio of solutes to recognition sites), and $\gamma = D_B/D_F$ (ratio of bound to free
- diffusivity of target solute).
- Each parameter in Eq. 5 is considered independently in an initial, simple analysis of the separation
- 15 factor. From the Stokes–Einstein relation, solute diffusivity and radius are inversely proportional,
- therefore $\delta = R_I/R_F$. To evaluate solubility, McMillan–Mayer solution theory⁶² is applied to
- determine the partitioning of a dilute solute species *i* between the external solution and the polymer
- 18 network:

$$S_i = \frac{[i]_{sol}}{[i]} = \exp\left(\frac{\Delta E_{ins}}{k_B T}\right)$$
 (6)

where ΔE_{ins} is the change in free energy upon insertion of a solute into the polymer network, k_B is the Boltzmann constant, and T is absolute temperature. Since the concentration of an equilibrated polymer network is proportional to that of a semi-dilute polymer solution,⁶³ the approach of de Gennes⁶⁴ and Odijk⁶⁵ is followed to consider the insertion of a non-interacting protein with radius R_p into a semi-dilute polymer solution with correlation length ξ_p . In the limit of $R_p < \xi_p$, known as the protein limit because most proteins exist in this size range, the free energy change is proportional to a depletion region formed around the protein:

$$8 \qquad \frac{\Delta E_{ins}}{k_B T} \cong \left(\frac{R_p}{\xi_p}\right)^{4/3} \tag{7}$$

9 resulting in the dependence of σ on solute size:

11

12

13

14

15

16

17

18

19

20

21

10
$$\sigma = \exp\left[\left(\frac{R_I}{\xi_p}\right)^{4/3} - \left(\frac{R_F}{\xi_p}\right)^{4/3}\right]$$
 (8)

To simplify calculations and illustrate the potential specificity of this approach, the following analysis is restricted to the separation of equally sized target and inert protein solutes ($R_F = R_I$). This mathematically straightforward case ($\delta = \sigma = 1$) represents the most chemically and physically challenging of separations. This case also holds biological significance, as natural filtration systems routinely separate proteins of similar size and shape. For example, nuclear pore complexes preferentially translocate nuclear transport receptors (NTF2 dimer, 29 kDa, 2.50 nm hydrodynamic radius) in comparison to inert reference molecules such as green fluorescent protein (GFP, 28 kDa, 2.35 nm hydrodynamic radius). Moreover, fusion proteins containing monomeric β -barrel fluorescent proteins mCherry or GFP (67 or 75 kDa fusions with estimated hydrodynamic radii of 2.96 or 3.18 nm, respectively)⁶⁶ have been selectively separated by biosynthetic hydrogels derived from the *S. cerevisiae* nucleoporin protein Nsp1.^{36, 39}

1 A broad parameter space is identified for selective biomolecular transport, illustrated as the target-2 to-inert protein flux ratio given constant γ or β (Figures 2a-b, respectively). Both plots include the parameter set $\gamma = \beta = 10^{-3}$ (green). In all cases, the target-to-inert flux ratio increases monotonically 3 with K_{eq} . Figure 2a suggests that excess polymer recognition sites are required for selective 4 filtration to occur. As recognition site availability is reduced ($\beta \rightarrow 0$), selective filtration 5 performance plateaus, where $(J_B+J_F)/J_I \rightarrow \sigma^2\delta(2+K_{eq}\gamma)$. The black dotted line indicates the 6 7 physical limit of infinite recognition sites in the polymer network. Figure 2b suggests that 8 significant bound-state diffusivity is required for selective separation of a biomolecular solute. The 9 black dotted line indicates the upper limit of passive, non-facilitated solute transport, in which 10 bound-state motions occur at the same rate as free-solution diffusion.

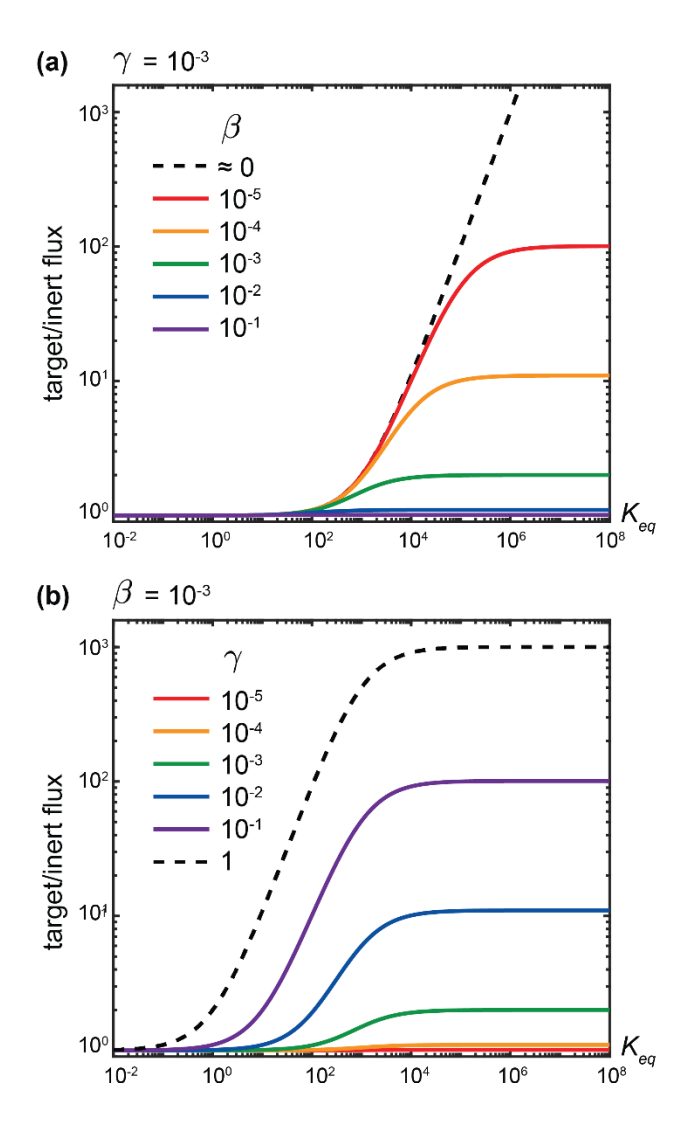


Figure 2. Target-to-inert protein flux ratios suggest optimal dimensionless parameters K_{eq} , β , and γ for the design of selectively permeable polymer networks. $\delta = \sigma = 1$. (a) and (b) illustrate constant γ and β , respectively, with the shared curve $\gamma = \beta = 10^{-3}$ (green). Black dashed curves indicate the physical limits of (a) infinite solute dilution ($\beta \rightarrow 0$) and (b) maximum bound diffusivity ($\gamma \rightarrow 1$). Selective permeability of biomolecules with multiple receptors. Although this initial analysis treats all transport and kinetic parameters through the polymer gel as independent, these parameters are in fact constrained by molecular processes. In particular, the bound-state diffusivity D_B depends on the existence of multiple bound states and the transition rates between these states. To

- investigate these transitions, consider a biomolecule M with a number of binding receptors N_B .
- 2 Multiple binding receptors are commonly displayed on the surfaces of biomolecules of interest,
- 3 including nuclear transport receptors, ^{17, 67} immunoglobulins, ^{68, 69} and broad classes of biological
- 4 toxins. $^{1, 2, 70, 71}$ Upon binding with the polymer network, M may exist in one of N_B bound states:

- 6 where receptor association rate constant k_{01}^* is identical to the continuum association rate constant
- 7 k_{on}^* from the two-state model. In the two-state model, molecules in all of the bound states $M_{j\geq 1}$ are
- 8 lumped into the single continuum bound state B. The receptor dissociation rate scales with the
- 9 continuum dissociation rate as follows:

$$10 k_{10} = \frac{[B]}{[M_1]} k_{off} (10)$$

- 11 Binding sites are assumed as equivalent, and each binding event is assumed to occur
- independently. Specifically, a molecule in state M_i must enter state M_{i+1} before M_{i+2} , and vice
- versa. Association rate constants k_{01}^* , k_{12}^* , etc. are considered equal and hereafter denoted k_{on}^* .
- 14 Similarly, equivalent dissociation rates k_{10} , k_{21} , etc. are designated k'_{off} , and the receptor
- equilibrium binding constant is K'_{eq} .
- 16 The continuum dissociation rate k_{off} excludes intermediate unbinding events and describes only
- transitions to the fully unbound state M_0 :

18
$$[B]k_{off} = [M_1]k_{10} = [M_1]k'_{off}$$
 (11)

19 such that the receptor dissociation rate scales as:

$$k'_{off} = \frac{[B]}{[M_1]} k_{off}$$
 (12)

Two distinct molecular motions arise from unbinding events: hopping and walking. During a hopping event, a singly bound molecule M_1 enters the free state M_0 . Here, biomolecular motion is governed by the solution diffusion coefficient D_F and does not contribute to bound-state diffusivity. During a walking event, a molecule in state $M_{j>1}$ unbinds, takes a "step" by changing position in a lesser bound state M_{j-1} , and re-binds elsewhere (**Figure 3a**).¹⁸⁻²⁰ Although multi-point biomolecular attachment results in caging, the cage itself changes shape and diffuses by releasing one or more of the attached points. This walking mechanism is distinct from directed motion observed in processive enzymes and translocation motors, both of which require mechanochemical cycling.¹⁰

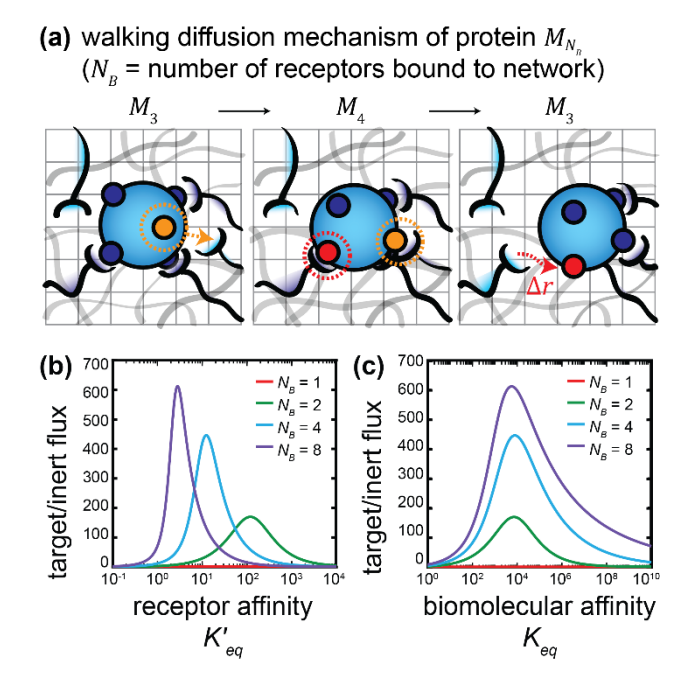


Figure 3. Walking diffusion enables selective transport of multivalent biomolecules. (a) Sequential binding (orange) and unbinding (red) events of a multi-receptor protein M_{N_B} in an interacting polymer network. This series of events results in walking diffusion, such that the solute center-of-mass position changes by step size Δr . Target biomolecular solute flux greatly exceeds

- inert flux as the number of receptors N_B increases, shown with respect to the equilibrium binding
- 2 constants of (b) single receptors K'_{eq} and (c) collective biomolecules K_{eq} .
- 3 In order to determine the step size, consider a polymer network with a characteristic length R
- 4 between biomolecular recognition sites and network junctions. The maximum distance that a
- 5 solute can move during a walking event is $\langle R^2 \rangle / (j-1)$, where (j-1) receptors remain attached to the
- 6 network during the step.²⁰ The bound diffusivity is expressed as:

$$D_B = \sum_{j=2}^{N_B} k'_{off} P_j \left(\frac{\langle R^2 \rangle}{j-1}\right)$$
 (13)

8 where P_j is the probability of state M_j . P_j follows a binomial distribution of receptor states:

$$P_{j} = \binom{N_{B}}{j} p_{B}^{j} p_{F}^{N_{B}-j} \tag{14}$$

- where receptor probabilities $p_B = K'_{eq}/(1 + K'_{eq})$ and $p_F = 1/(1 + K'_{eq})$ are determined from
- an equilibrium material balance. The presence of multiple binding receptors in M and specification
- of walking diffusion as the bound state mechanism result in modified expressions β and γ :

$$\beta = N_B \frac{[F]_{sol}}{[S]} \tag{15}$$

14
$$\gamma = \frac{k'_{off} \langle R^2 \rangle}{D_F} \sum_{j=2}^{N_B} \frac{P_j}{j-1}$$
 (16)

- 15 The target-to-inert flux ratio is re-written as a function of measurable physical parameters (e.g.
- biomolecular radii, binding rate constants, and polymer network properties):

17
$$\frac{\text{target flux}}{\text{inert flux}} = \frac{J_B + J_F}{J_I} = \delta \sigma^2 \left(\frac{1 + \omega K'_{eq} N_B \frac{[F]_{SOl}}{[S]} + \frac{\omega k^*_{eq} N_B \frac{[F]_{SOl}}{D_F}}{D_F} \sum_{j=2}^{N_B} \frac{P_j}{j-1}}{1 + \omega K'_{eq} N_B \frac{[F]_{SOl}}{[S]}} \right)$$
(17)

- where receptor scaling factor $\omega = (\sum_{j=1}^{N_B} P_j)/P_1 = K_{eq}/K'_{eq}$. Following the incorporation of
- 19 explicit bound-state walking diffusion, the separation of multi-receptor biomolecular solutes by

polymer membranes with varying interactions can be predicted by estimating molecular parameters from selective transport experiments with nucleoporin-like proteins (Figures 3b-c):³⁹ $[F]_{sol} = 5 \mu M$ from transport receptor protein solutions; [S] = 70 mM from 20% w/v protein hydrogels, wherein each protein molecule (46 kDa) has 16 phenylalanine-glycine binding sites; $k_{on} = 1.5 \times 10^9 \text{ M}^{-1} \text{ s}^{-1}$ from theoretical predictions and experimental measurements of nuclear transport receptor association rates; 72,73 $D_F = 4.4 \times 10^{-11}$ m² s⁻¹ from the Stokes–Einstein relation of a protein in water $(R_p = 5 \text{ nm})$; and $\langle R^2 \rangle = \langle (5 \text{ nm})^2 \rangle$ from the Flory radius of a natively unfolded nucleoporin protein, ^{74,75} which approximates the distance between recognition sites and crosslinks in an intrinsically disordered polymer network. These parameters serve primarily as a starting point to understand the key factors underlying selective transport phenomena.

In all cases with multiple receptors, selective permeability depends non-monotonically on affinity, and selective transport occurs over a broad range of binding affinities. As the number of binding receptors N_B increases, the optimal affinity for an individual receptor decreases; however, selective transport performance does not depend strongly on binding site number when rescaled according to molecular-scale K_{eq} . The optimal two-state binding equilibrium constant K_{eq} is consistently between 10^3 and 10^4 . This macroscopic affinity corresponds to biomolecular dissociation constants K_d between 10 and 100 μ M, which are consistent with experimentally determined constants for nuclear transport receptors $(1-100 \ \mu\text{M})$. Beyond this range, the separation factor is more sensitive to weak recognition than strong interactions (note the logarithmic scale).

These results suggest how walking mechanisms can enable selective biomolecular transport.

Unbound impurity and filtrate molecules, which have the same diffusivity and solubility in the free state of the polymer network, have equal permeability. However, binding of a biomolecular target dramatically increases its concentration. The ability of bound state molecules to cross the polymer

- 1 gel, even slowly, leads to enhanced permeation of the desired biomolecules. Solutes with more
- 2 receptors favor walking, and a binding coefficient that is too strong reduces mobility. In contrast,
- 3 binding that is too weak decreases the bound-state concentration.
- 4 Model-Driven Design of Gels for Recognition And Selective Permeation. GRASP was 5 engineered to realize the key features of the two-state model, entropic repulsion and affinity 6 interactions, in a synthetic material that exhibits permeability to a specific biomolecular target. 7 Biomimicry of the nuclear pore was approached by copying the simplest diffusion mechanism in 8 order to produce the same macroscopic response of selective transport in a hydrogel. To this end, 9 GRASP was designed as a crosslinked poly(ethylene glycol) (PEG) network with embedded 10 protein-binding oligopeptides. The introduction of numerous binding sites within the network 11 mimics the presence of numerous FG domains in a nucleoporin protein matrix. Oligopeptides 12 consist of a tunable binding region flanked by glycine spacers and cysteine residues for 13 bioconjugation at both termini. PEG was chosen for its low-protein-adsorption properties, versatile conjugation functionalities, and commercial availability.^{53, 76} A series of PEG-peptide networks 14 15 were synthesized by simultaneous conjugation and polycondensation of tetra-PEG-maleimide and 16 di-cysteine peptides (Figure 4a). This approach is general to peptides that do not contain native cysteine, which includes the antigenic epitopes for many commercial monoclonal antibodies. 77,78 17

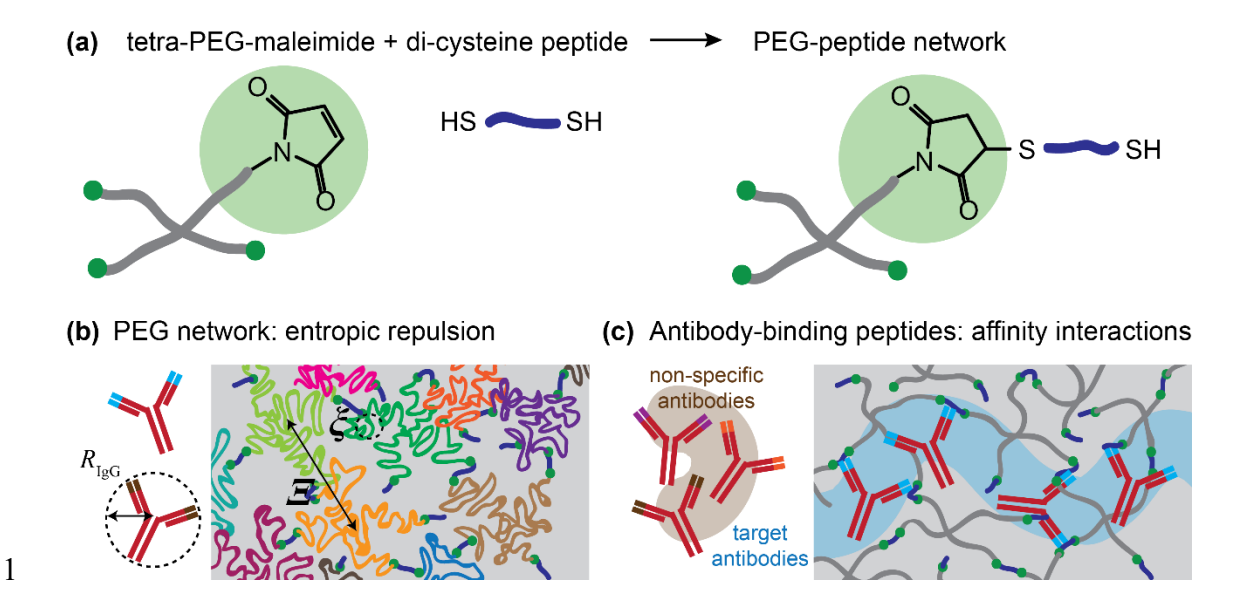


Figure 4. GRASP design for antibody separations. (a) Thiol-maleimide coupling chemistry

3 enables simultaneous bioconjugation and crosslinking of PEG-peptide networks. (b) Space-filling 4 schematic of entropic repulsion by polymers forming hydrogel networks. Different colors 5 represent individual tetra-PEG molecules. Network junctions form a dynamic mesh (Ξ), but non-6 specific antibodies of radius R_{IgG} are excluded by polymer correlations (ξ). (c) Topological 7 schematic of affinity interactions with peptide domains, which allow transport of targeted peptide-8 interacting antibodies through the polymer network. 9 The ideal targets for this study would have distinct, well-defined binding behavior while exhibiting 10 a high degree of similarity between other physicochemical properties. Such targets are biologically significant, as natural filtration systems routinely separate proteins of similar size and shape. 14, 34-11 ⁴⁰ Immunoglobulin G (IgG) antibodies naturally possess these features and were selected as model 12 13 biomolecules for the design and development of GRASP. In particular, anti-c-Myc IgG exhibits known interactions with various peptide sequences derived from the c-Myc protein, 52 enabling a 14 systematic study of the impact of binding behavior on anti-c-Myc IgG permeability in synthetic 15 16 PEG-peptide networks. Moreover, bivalency is a minimal physical criterion for walking diffusion,

- and IgG antibodies have two symmetric binding sites that enable a strong proof-of-concept for
- 2 walking diffusion in selectively permeable hydrogels.
- 3 PEG precursors were selected to form a network with two length scales suitable for IgG separations
- 4 (**Figure 4b**). Local polymer correlations result in a smaller correlation length ξ , which depends on
- 5 polymer chemistry and solvent quality. 63 At this length scale, the excluded volume of the polymer
- 6 network repels non-specific biomolecules. The physical separation between crosslink junctions
- 7 forms a larger correlation length Ξ , which depends on the molecular weight of the adjoining
- 8 polymer strand. This dynamic mesh size allows molecules with enhanced permeability to pass
- 9 through the network.⁷⁹⁻⁸¹
- 10 IgG-GRASP interactions can be modulated by oligopeptide binding domain sequence, and IgG
- fulfills the two-receptor minimum required for biomolecular walking (Figure 4c). A GRASP
- series was synthesized using peptides with varying affinity interactions with (0.56 μ M < K_d < 200
- 13 μ M, **Table 1**), where K_d is the peptide dissociation constant with anti-c-Myc monoclonal antibody
- 14 (9E10).⁵² It should be noted that K_d is the dimensional inverse of K_{eq} from the two-state model,
- such that $K_d = \frac{k_{off}[S]}{k_{on}} = \frac{k_{off}[S]}{k_{on}[S]} = \frac{k_{off}[S]}{k_{on}^*} = \frac{[S]}{K_{eq}}$. The GRASP series also included a non-binding
- 16 control peptide with the sequence CGGC.

Table 1. Physical properties of c-Myc (9E10) peptide-conjugated GRASP

1

c-Myc (9E10) peptide (*epitopes ⁵² in blue)	$K_d (\mu M)^{52}$	G'(kPa)*	Conversion (%)*	ζ (nm)**
CGGEQKLISEEDLGGC	0.56 ± 0.19	1.3 ± 0.1	68 ± 1	1.2 ± 0.1
CGGKLISEFELGGC	7.3 ± 0.56	0.8 ± 0.0	65 ± 0	1.3 ± 0.1
CGGKLISEEDLGGC	26 ± 19	2.0 ± 0.3	72 ± 2	1.5 ± 0.1
CGGQLISEEDLGGC	82 ± 43	2.6 ± 0.5	76 ± 3	1.0 ± 0.1
CGGKLISDEDLGGC	> 200	2.0 ± 0.1	72 ± 1	1.2 ± 0.1
CGGC	N/A	2.1 ± 0.3	73 ± 2	1.5 ± 0.1

^{*}mean ± standard deviation; **95% confidence interval of non-linear least squares fit

- 3 Shear Rheology and Gel Conversion. Highly reproducible measurements of the shear elastic and
- 4 viscous moduli (G' and G'', respectively) were achieved across three replicates of each sample. In
- each GRASP, G' was independent of frequency and larger than G'' (Figure S1), which is consistent
- 6 with the expected elastic solid behavior of chemically crosslinked polymer networks. Variations
- 7 in G' and conversion across the GRASP series are attributed to different oligopeptide sequences,
- 8 which are known to affect thiol-maleimide conjugation efficiency. 53,76
- 9 The conversion of GRASP gelation by bioconjugation and polycondensation reactions was
- 10 estimated using the elastic shear modulus and a gel-point model based on a modified phantom
- network theory (details in SI),⁸² which describes how loop defects affect bulk elasticity in gels.
- 12 Chemically crosslinked gels are susceptible to the formation of topological defects such as
- dangling ends, primary loops, and high-order cyclic defects.^{54, 82-85} Topological defects suppress
- gelation⁸⁶ and decrease the mechanical properties of gels.⁸² Gels synthesized using A₂ + B₄
- functionalities, such as GRASP, are particularly susceptible to cyclic defects.⁵⁴

Entropic Repulsion of Non-Specific Biomolecules. Selective permeation by GRASP requires the rejection of non-specific proteins with an entropic barrier. In polymer gels and networks, local polymer interactions result in a correlation length ξ that depends on polymer chemistry and solvent quality.⁶³ At this scale, the excluded volume of the polymer forms an entropic mesh that hinders the motion of non-specific macromolecules and particles larger than ξ .^{79-81, 87, 88} The entropic meshes formed in PEG–peptide networks were characterized using SANS. The reduced scattering intensity *I* as a function of scattering vector *q* was fit to a correlation length model:^{56, 58}

where multiplicative factors A and C and exponents m and n are related to the Porod and Lorentzian

exponents, respectively. B is incoherent scattering from the background. Fitting by non-linear

8
$$I(q) = \frac{A}{q^m} + \frac{C}{1 + (q\xi)^n} + B$$
 (18)

least-squares regression in MATLAB resulted in ξ measurements between 1.0 and 1.5 nm for each GRASP (**Table 1**, **Figure S2**). These mesh sizes are sufficiently small to reject IgG molecules, which have hydrodynamic radii of approximately 5.4 nm.⁸⁹ Similar correlation lengths across the GRASP series reflects the minimal effect of different peptide sequences on the entropic barrier.

Despite size exclusion by entropic repulsion, GRASP allows selective transport of proteins with dimensions greater than the measured correlation lengths. Meshes and size exclusion cutoffs are fixed in rigid materials; however, a dynamic mesh size Ξ emerges from heterogeneity, elasticity, and thermal fluctuations in polymer networks.⁷⁹⁻⁸¹ This larger mesh size is equal to the physical separation between crosslinking junctions, which is also the Flory radius of the adjoining polymer strand. In GRASP, crosslink junctions are formed at the centers of tetra-arm PEG molecules, such that a strand between junctions consists of an oligopeptide and two PEG arms (5 kDa molecular weight per arm). For hydrated 10 kDa PEG strands, Ξ is calculated as 10.0 nm, ⁹⁰ which exceeds

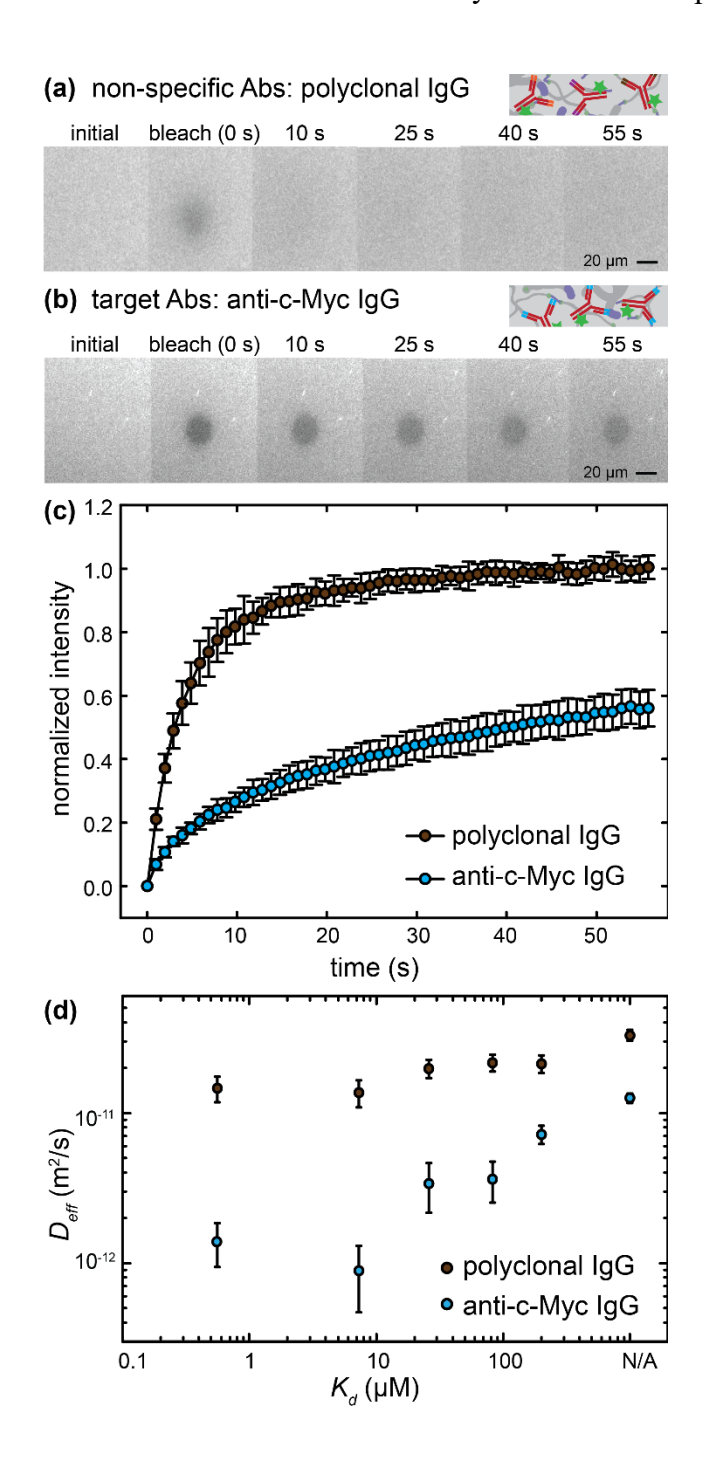
- 1 the 5.4 nm hydrodynamic radius of IgG.⁸⁹ Therefore, IgG antibodies that are targeted by peptide
- 2 affinity interactions can overcome entropic repulsion and exhibit enhanced hydrogel permeation.
- 3 Affinity-Mediated Permeability Enabled by Bound-State Antibody Diffusion. FRAP and 1D
- 4 transport assays were applied to characterize the diffusivity, permeability, and selectivity of
- 5 antibodies in each GRASP. The lateral diffusion of fluorescein isothiocyanate (FITC)-labeled anti-
- 6 c-Myc IgG and polyclonal IgG were compared after equilibration in PEG-peptide networks with
- 7 varying peptide affinities. Figure 5a-b shows time-lapsed confocal microscope images of non-
- 8 specific polyclonal IgG and targeted anti-c-Myc IgG in a strongly interacting hydrogel ($K_d = 0.56$
- 9 μM). Raw experimental FRAP images were converted into normalized fluorescence intensity
- 10 curves (Figure 5c) using double and full-scale normalization⁹¹ to enable quantitative analysis and
- 11 comparison across samples. This method utilizes three regions of interest (bleached spot, non-
- bleached background, and non-fluorescent background) to correct for variations in the pre-bleach
- signal, the loss of total signal during acquisition, and laser intensity fluctuations. Normalized
- intensity curves I(t) were fit using non-linear least squares regression in MATLAB according to
- 15 the closed form solution for diffusion in a circular spot:²⁹

$$I(t) = Ae^{-\frac{\tau_D}{2t}} \left[I_0 \left(\frac{\tau_D}{2t} \right) + I_1 \left(\frac{\tau_D}{2t} \right) \right] \tag{19}$$

- where A is a fitting parameter related to the mobile and bound fraction of biomolecules, I_0 and I_1
- are modified Bessel functions of the first kind, and τ_D is a characteristic diffusion time. Fits of all
- 19 experimental data for non-interacting polyclonal IgG and interacting anti-c-Myc IgG are shown in
- Figures S3 and S4, respectively. The effective diffusivity D_{eff} is calculated according to the
- 21 following relation:

$$D_{eff} = w^2 / \tau_D \tag{20}$$

- where w is the radius of the bleached spot (14 μ m). D_{eff} reflects an average measurement of all
- 2 diffusive mechanisms exhibited by a biomolecular population.



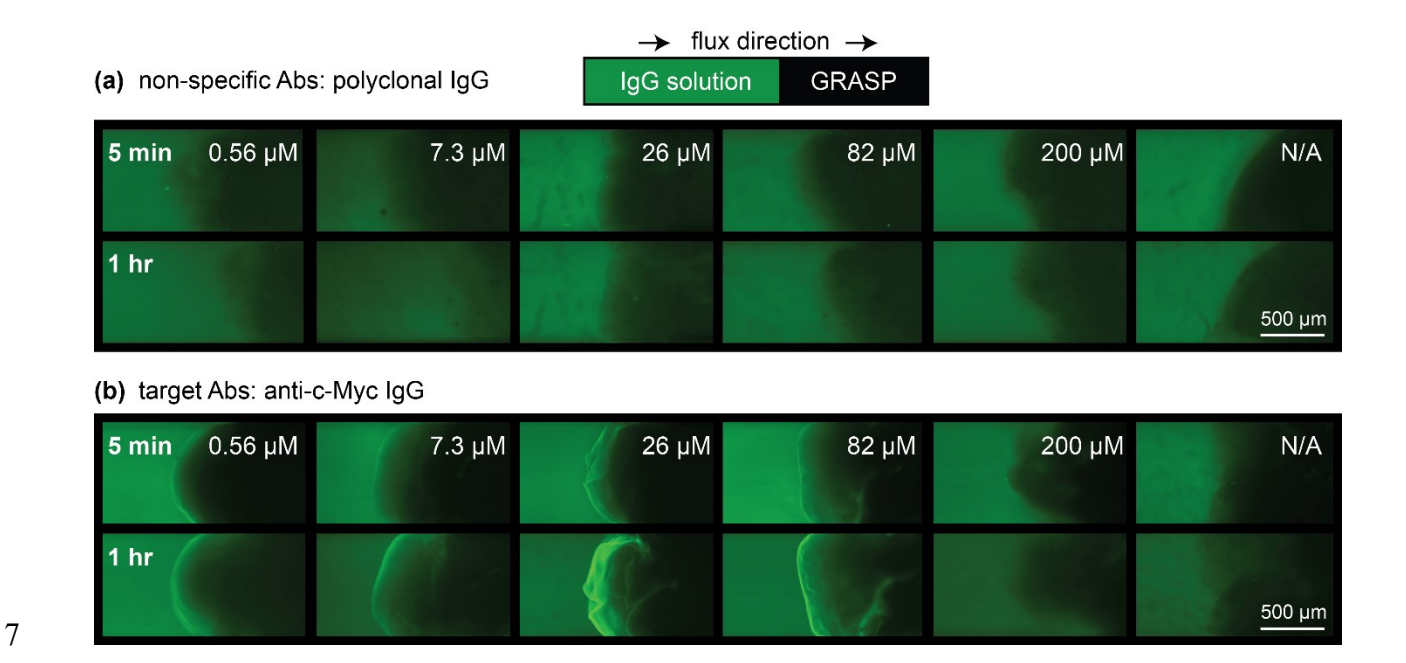
3

4 Figure 5. Interacting antibodies exhibit reduced diffusivity in GRASP. (a) Time-lapse images

5 from FRAP experiments of (a) polyclonal IgG-FITC and (b) anti-c-Myc IgG-FITC in the same

- 1 hydrogel ($K_d = 0.56 \mu M$) are converted into (c) normalized intensity with respect to time. (d)
- 2 Diffusivity (mean \pm st. dev.) of anti-c-Myc and polyclonal IgG-FITC in a GRASP series with
- 3 varying affinity interactions.
- 4 The diffusivity of non-specific IgG remained relatively unchanged across the GRASP series
- 5 (Figure 5d). Using the Stokes–Einstein relation, the free diffusivity of IgG in water is estimated
- as 4.0×10^{-11} m²/s ($R_{\rm IgG} = 5.4$ nm), ⁸⁹ which is comparable to the measured diffusivity of polyclonal
- 7 IgG $(2.1 \pm 1.0 \times 10^{-11} \text{ m}^2/\text{s})$ in PEG-peptide networks. The diffusivity of polyclonal IgG suggests
- 8 that non-binding biomolecules only exist in the unbound, freely diffusing biomolecular state,
- 9 wherein antibodies do not undergo affinity interactions with the gel. The diffusion of non-specific
- 10 polyclonal IgG also suggests that PEG-peptide networks have pores that are sufficiently large for
- 11 the selective permeation of anti-c-Myc IgG.
- 12 Anti-c-Myc IgG diffused more slowly than polyclonal IgG in all hydrogels. In the negative control
- gel, anti-c-Myc IgG diffusivity was comparable to the average diffusivity of polyclonal IgG. As
- oligopeptide domain affinity increased, anti-c-Myc IgG diffused more slowly, indicating a larger
- bound fraction or slower bound state diffusivity via the walking mechanism. The combination of
- a large subpopulation of bound-state biomolecules with non-zero bound-state diffusivity can lead
- 17 to enhanced biomolecular permeability in a polymer network, despite a reduction in the average
- 18 diffusivity.
- 19 GRASP permeability was evaluated using 1D fluorescence transport assays in a semi-infinite slab
- 20 geometry.^{39, 40} Briefly, borosilicate capillaries were partially filled with hydrogels, and
- 21 fluorescently labeled antibody solutions were introduced to the exposed interfaces. Antibody
- 22 diffusion across each buffer-GRASP interface was observed using fluorescence microscopy.

- 1 Solutions containing polyclonal IgG or anti-c-Myc IgG (Figures 6a-b, respectively) were tested
- 2 separately. Transport of anti-c-Myc IgG across the interface was observed in hydrogels with 0.56
- 3 μ M < K_d < 82 μ M, as indicated by the development of an intense fluorescent band at the GRASP–
- 4 buffer interface. In contrast, weakly interacting ($K_d = 200 \mu M$) and negative control hydrogels
- 5 exhibited a slab diffusion profile with no enhanced binding or transport of anti-c-Myg IgG at the
- 6 interface. In all hydrogels, non-specific polyclonal IgG exhibited only a slab diffusion profile.



8 Figure 6. 1D transport assays reveal (a) entropic repulsion of non-specific polyclonal IgG-FITC

9 by each GRASP and (b) non-monotonic affinity-mediated permeation of anti-c-Myc IgG-FITC.

10

11

12

13

14

Anti-c-Myc IgG exhibited non-monotonic permeability with respect to K_d , consistent with predictions of the two-state transport model. Anti-c-Myc IgG also exhibited the greatest enhancement in permeation through hydrogels with intermediate K_d (26 and 82 μ M), supporting the notion of molecular walking during selective transport. Despite the distinct chemistry and structure of GRASP in comparison to nuclear pore proteins, the macroscopically observable

- 1 feature of selective permeability to anti-c-Myc IgG over polyclonal IgG is remarkably similar to
- 2 the response of selectively permeable nucleoporin-based hydrogels to nuclear transport
- 3 receptors.³⁵⁻⁴¹
- 4 GRASP selectivity was measured using transport assays with two-color fluorescence microscopy
- 5 (Figure 7a). Antibody solutions consisted of a mixture of anti-c-Myc IgG-FITC (green) and
- 6 polyclonal IgG-Alexa Fluor® 594 (red). The GRASP-buffer interface was identified using bright-
- 7 field imaging to measure distance-dependent fluorescent intensity profiles (**Figures 7b-c**), which
- 8 were normalized to the intensity of the reservoir buffer. The selectivity of each GRASP was
- 9 quantified by the ratio of maximum normalized intensities between anti-c-Myc IgG and polyclonal
- 10 IgG (**Figure 7d**). Selective anti-c-Myc IgG permeability exceeded the performance estimated by
- the two-state model, which predicts a maximum selective antibody flux ratio of 1.7 (details in SI).
- 12 The model suggests that antibody transport is particularly challenging due to limited binding sites
- and strong binding affinities, especially in comparison to multivalent, low-affinity nuclear
- 14 transport receptors. Interestingly, GRASP exhibited approximately 3-fold increases in selective
- anti-c-Myc IgG permeability in comparison to non-selective controls. GRASP transport properties
- are easily tuned by careful selection of peptide and PEG domains, presenting an opportunity to
- design versatile materials that control selective biomolecular transport.

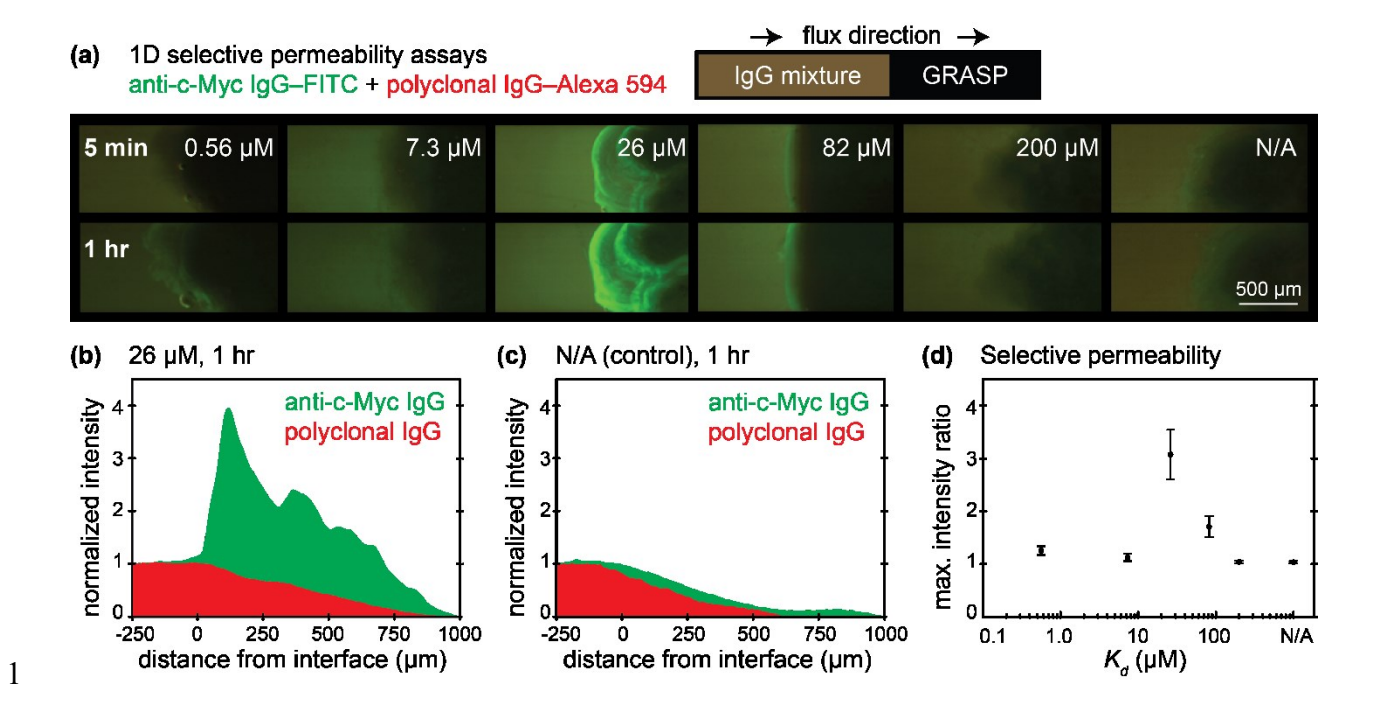


Figure 7. Selective permeability of GRASP. (a) Representative series of transport assays with anti-c-Myc IgG (green) and polyclonal IgG (red). (b,c) Normalized fluorescence intensity profiles for selective ($K_d = 26 \mu M$) and non-selective hydrogels. (d) Selective permeability (mean \pm standard error) is non-monotonic with respect to IgG–GRASP affinity.

6 Conclusions

Nucleopore-inspired hydrogels are designed and synthesized following key principles uncovered by a molecular transport theory that predicts how binding interactions to a stationary polymer gel can accelerate passive molecular transport: (1) entropic repulsion of undesired biomolecules and (2) affinity-mediated permeability of target biomolecules through a walking diffusion mechanism. To implement these principles in a novel material, Gels for Recognition And Selective Permeation were designed, consisting of a polyethylene glycol network containing numerous oligopeptide binding domains with selective affinity for a monocolonal antibody. The entropic barriers formed

- by PEG networks limit protein transport, while oligopeptide recognition by the antibody allows
- 2 selective transport of one monoclonal antibody from a polyclonal set.
- 3 Experiments and theory both demonstrate a non-monotonic effect of affinity interactions on
- 4 GRASP transport properties. Strong affinity interactions prevent walking mechanisms that allow
- 5 biomolecular transport in polymer networks, whereas weak affinity interactions prevent target
- 6 biomolecules from overcoming the entropic barrier of GRASP. A two-state molecular transport
- 7 theory suggests a broad parameter space for materials with selective transport properties, which
- 8 can be enhanced by increasing the valence of target biomolecules.
- 9 The use of multivalent receptors is a well-known biological strategy for transport, not only by
- nuclear transporters but also biological toxins, 1,2 nucleic-acid-binding proteins, 92,93 and clustered
- transmembrane receptors. 94 Application of the two-state transport model will guide the design of
- synthetic polymer membranes that replicate, if not enhance, the ability of biological membranes
- 13 to control molecular transport. In this way, GRASP provides a platform for the rational design of
- 14 versatile materials to regulate the detection, delivery, and separation of biomolecules, which could
- broadly influence applications including the production of biopharmaceutical targets, treatment of
- 16 contaminated water and food, and development of synthetic anti-toxin materials.

17 ASSOCIATED CONTENT

- 18 Supporting Information. Details of the two-state model, including dimensional analysis, the full
- analytical solution of linearized, steady-state transport through a 1D membrane, and molecular
- 20 parameters used to estimate GRASP performance. Gel conversion calculations using RENT.
- 21 Additional data from rheological characterization, SANS, and FRAP.

AUTHOR INFORMATION

- 2 Corresponding Author
- 3 E-mail: bdolsen@mit.edu
- 4 ORCID

- 5 Yun Jung Yang: 0000-0003-0684-5218
- 6 Danielle J. Mai: 0000-0001-5447-2845
- 7 Thomas J. Dursch: 0000-0002-9414-6478
- 8 Bradley D. Olsen: 0000-0002-7272-7140
- 9 **Author Contributions**
- [†]Y.J.Y. and D.J.M. contributed equally to this work. Y.J.Y., D.J.M., and B.D.O. conceived the
- project, analyzed data, and wrote the manuscript. D.J.M., T.J.D., and B.D.O. developed the
- transport model. Y.J.Y. performed GRASP synthesis and characterization (SAOS, FRAP, and
- transport assays).
- 14 Notes
- 15 The authors declare no competing financial interests.
- 16 ACKNOWLEDGMENTS
- 17 This work was supported by the Defense Threat Reduction Agency under contract HDTRA1-13-
- 18 1-0038 and the National Science Foundation (CBET 1705923). D.J.M. acknowledges support from
- 19 the Arnold and Mabel Beckman Foundation. A portion of this research used resources at the
- 20 Spallation Neutron Source and High Flux Isotope Reactor (HFIR), DOE Office of Science User
- Facilities operated by the Oak Ridge National Laboratory. We thank C. E. Mills and H. Yao for

- 1 conducting SANS experiments, as well as S. Qian (HFIR Bio-SANS CG-3) for guidance through
- 2 preliminary SANS experiments. We also thank R. Wang, M. K. Sing, R. K. Avery, and T.-S. Lin
- 3 for helpful discussions.

4 ABBREVIATIONS

- 5 GRASP, Gel for Recognition And Selective Permeation; FG, phenylalanine-glycine; FITC,
- 6 fluorescein isothiocyanate; FRAP, fluorescence recovery after photobleaching; IgG,
- 7 immunoglobulin G; NTR, nuclear transport receptor; NPC, nuclear pore complex; PEG,
- 8 poly(ethylene glycol); SANS, small-angle neutron scattering.

9 **REFERENCES**

- 10 1. Parker, M. W.; Feil, S. C., Pore-forming protein toxins: from structure to function. *Prog. Biophys. Mol. Biol.* **2005**, 88, (1), 91-142.
- 2. Beddoe, T.; Paton, A. W.; Le Nours, J.; Rossjohn, J.; Paton, J. C., Structure, biological functions and applications of the AB5 toxins. *Trends Biochem. Sci.* **2010,** 35, (7), 411-
- 14 418.
- 15 3. Xu, L.; Lee, H.; Pinheiro, M. V. B.; Schneider, P.; Jetta, D.; Oh, K. W., Phaseguide-
- assisted blood separation microfluidic device for point-of-care applications.
- 17 *Biomicrofluidics* **2015**, 9, (1), 014106.
- 18 4. Du, K.; Park, M.; Griffiths, A.; Carrion, R.; Patterson, J.; Schmidt, H.; Mathies, R.,
- Microfluidic System for Detection of Viral RNA in Blood Using a Barcode Fluorescence
- Reporter and a Photocleavable Capture Probe. Anal. Chem. 2017, 89, (22), 12433-12440.
- 5. Schwartz, J.; Padmanabhan, A.; Aqui, N.; Balogun, R. A.; Connelly-Smith, L.; Delaney,
- M.; Dunbar, N. M.; Witt, V.; Wu, Y.; Shaz, B. H., Guidelines on the Use of Therapeutic
- 23 Apheresis in Clinical Practice–Evidence-Based Approach from the Writing Committee of
- the American Society for Apheresis: The Seventh Special Issue. J. Clin. Apheresis 2016,
- 25 31, (3), 149-338.
- 26 6. Follman, D. K.; Fahrner, R. L., Factorial screening of antibody purification processes
- using three chromatography steps without protein A. J. Chromatogr. A **2004**, 1024, (1–2),
- 28 79-85.
- 29 7. Gottschalk, U., Bioseparation in Antibody Manufacturing: The Good, The Bad and The
- 30 Ugly. Biotechnol. Prog. 2008, 24, (3), 496-503.

- 1 8. Ladisch, M. R., *Bioseparations engineering: principles, practice, and economics.* Wiley: 2001.
- 9. Rivas, G.; Minton, A. P., Macromolecular Crowding In Vitro, In Vivo, and In Between. 4 *Trends Biochem. Sci.* **2016**, 41, (11), 970-981.
- 5 10. Elston, T. C., A macroscopic description of biomolecular transport. *J. Math. Biol.* **2000**, 41, (3), 189-206.
- 7 11. Agarwal, A.; Hess, H., Biomolecular motors at the intersection of nanotechnology and polymer science. *Prog. Polym. Sci.* **2010**, 35, (1), 252-277.
- 9 12. Lieleg, O.; Ribbeck, K., Biological hydrogels as selective diffusion barriers. *Trends Cell Biol.* **2011**, 21, (9), 543-551.
- 13. Görlich, D.; Kutay, U., Transport between the cell nucleus and the cytoplasm. *Annu. Rev. Cell Dev. Biol.* **1999**, 15, 607-660.
- 13 14. Ribbeck, K.; Görlich, D., Kinetic analysis of translocation through nuclear pore complexes. *EMBO J.* **2001,** 20, (6), 1320-1330.
- 15. Cook, A.; Bono, F.; Jinek, M.; Conti, E., Structural biology of nucleocytoplasmic transport. *Ann. Rev. Biochem.* **2007**, 76, 647-71.
- Walde, S.; Kehlenbach, R. H., The Part and the Whole: functions of nucleoporins in nucleocytoplasmic transport. *Trends Cell Biol.* **2010**, 20, (8), 461-469.
- 19 17. Isgro, T. A.; Schulten, K., Binding Dynamics of Isolated Nucleoporin Repeat Regions to Importin-β. *Structure* **2005**, 13, (12), 1869-1879.
- Vanden Broek, W.; Thompson, N. L., When Bivalent Proteins Might Walk Across Cell
 Surfaces. J. Phys. Chem. 1996, 100, (27), 11471-11479.
- Hsieh, H. V.; Thompson, N. L., Theory for measuring bivalent surface binding kinetics using total internal reflection with fluorescence photobleaching recovery. *Biophys. J.* **1994,** 66, (3, Part 1), 898-911.
- 26 20. Ramirez, J.; Dursch, T. J.; Olsen, B. D., A Molecular Explanation for Anomalous Diffusion in Supramolecular Polymer Networks. *Macromolecules* **2018**, 51, (7), 2517-2525.
- 29 21. Bayliss, R.; Ribbeck, K.; Akin, D.; Kent, H. M.; Feldherr, C. M.; Görlich, D.; Stewart, M., Interaction between NTF2 and xFxFG-containing nucleoporins is required to mediate nuclear import of RanGDP 1. *J. Mol. Biol.* **1999**, 293, (3), 579-593.
- Chaillan-Huntington, C.; Braslavsky, C. V.; Kuhlmann, J.; Stewart, M., Dissecting the Interactions between NTF2, RanGDP, and the Nucleoporin XFXFG Repeats. *J. Biol. Chem.* 2000, 275, (8), 5874-5879.

- 1 23. Bayliss, R.; Littlewood, T.; Strawn, L. A.; Wente, S. R.; Stewart, M., GLFG and FxFG
- Nucleoporins Bind to Overlapping Sites on Importin-β. J. Biol. Chem. **2002**, 277, (52),
- 3 50597-50606.
- 4 24. Wagner, Raphael S.; Kapinos, Larisa E.; Marshall, Neil J.; Stewart, M.; Lim, Roderick Y.
- 5 H., Promiscuous Binding of Karyopherinβ1 Modulates FG Nucleoporin Barrier Function
- and Expedites NTF2 Transport Kinetics. *Biophys. J.* **2015,** 108, (4), 918-927.
- 7 25. Amsden, B., Solute Diffusion within Hydrogels. Mechanisms and Models.
- 8 *Macromolecules* **1998,** 31, (23), 8382-8395.
- 9 26. Amsden, B., An Obstruction-Scaling Model for Diffusion in Homogeneous Hydrogels.
- 10 *Macromolecules* **1999**, 32, (3), 874-879.
- Lin, C.-C.; Metters, A. T., Hydrogels in controlled release formulations: Network design
- 12 and mathematical modeling. *Adv. Drug Delivery Rev.* **2006**, 58, (12), 1379-1408.
- 13 28. Liu, D. E.; Kotsmar, C.; Nguyen, F.; Sells, T.; Taylor, N. O.; Prausnitz, J. M.; Radke, C.
- J., Macromolecule Sorption and Diffusion in HEMA/MAA Hydrogels. *Ind. Eng. Chem.*
- 15 Res. **2013**, 52, (50), 18109-18120.
- 16 29. Sprague, B. L.; Pego, R. L.; Stavreva, D. A.; McNally, J. G., Analysis of Binding
- 17 Reactions by Fluorescence Recovery after Photobleaching. *Biophys. J.* **2004,** 86, (6),
- 18 3473-3495.
- 19 30. Beaudouin, J.; Mora-Bermúdez, F.; Klee, T.; Daigle, N.; Ellenberg, J., Dissecting the
- 20 Contribution of Diffusion and Interactions to the Mobility of Nuclear Proteins. *Biophys*.
- *J.* **2006,** 90, (6), 1878-1894.
- 31. Gavutis, M.; Lata, S.; Lamken, P.; Müller, P.; Piehler, J., Lateral Ligand-Receptor
- Interactions on Membranes Probed by Simultaneous Fluorescence-Interference
- 24 Detection. *Biophys. J.* **2005**, 88, (6), 4289-4302.
- 25 32. Tang, S.; Wang, M.; Olsen, B. D., Anomalous Self-Diffusion and Sticky Rouse
- Dynamics in Associative Protein Hydrogels. J. Am. Chem. Soc. 2015, 137, (11), 3946-
- 27 3957.
- 28 33. Rapp, P. B.; Omar, A. K.; Shen, J. J.; Buck, M. E.; Wang, Z.-G.; Tirrell, D. A., Analysis
- and Control of Chain Mobility in Protein Hydrogels. J. Am. Chem. Soc. 2017, 139, (10),
- 30 3796-3804.
- 31 34. Frey, S.; Richter, R. P.; Görlich, D., FG-Rich Repeats of Nuclear Pore Proteins Form a
- Three-Dimensional Meshwork with Hydrogel-Like Properties. *Science* **2006**, 314,
- 33 (5800), 815-817.
- 35. Frey, S.; Gorlich, D., A saturated FG-repeat hydrogel can reproduce the permeability
- properties of nuclear pore complexes. *Cell* **2007**, 130, (3), 512-523.

- 1 36. Frey, S.; Görlich, D., FG/FxFG as well as GLFG repeats form a selective permeability barrier with self-healing properties. *EMBO J.* **2009**, 28, (17), 2554-2567.
- 37. Ader, C.; Frey, S.; Maas, W.; Schmidt, H. B.; Görlich, D.; Baldus, M., Amyloid-like interactions within nucleoporin FG hydrogels. *Proc. Natl. Acad. Sci. U. S. A.* **2010,** 107, (14), 6281-6285.
- Labokha, A. A.; Gradmann, S.; Frey, S.; Hülsmann, B. B.; Urlaub, H.; Baldus, M.;
 Görlich, D., Systematic analysis of barrier-forming FG hydrogels from *Xenopus* nuclear pore complexes. *EMBO J.* 2013, 32, (2), 204-218.
- 9 39. Kim, M.; Chen, W. G.; Kang, J. W.; Glassman, M. J.; Ribbeck, K.; Olsen, B. D., Artificially Engineered Protein Hydrogels Adapted from the Nucleoporin Nsp1 for Selective Biomolecular Transport. *Adv. Mater.* **2015**, 27, (28), 4207-4212.
- 12 40. Kim, M.; Chen, W. G.; Souza, B. S.; Olsen, B. D., Selective biomolecular separation 13 system inspired by the nuclear pore complex and nuclear transport. *Mol. Syst. Des. Eng.* 14 **2017**, 2, (2), 149-158.
- Chen, W. G.; Witten, J.; Grindy, S. C.; Holten-Andersen, N.; Ribbeck, K., Charge
 Influences Substrate Recognition and Self-Assembly of Hydrophobic FG Sequences.
 Biophys. J. 2017, 113, (9), 2088-2099.
- 18 42. Tae, G.; Scatena, M.; Stayton, P. S.; Hoffman, A. S., PEG-cross-linked heparin is an affinity hydrogel for sustained release of vascular endothelial growth factor. *J. Biomater.* 20 Sci., Polym. Ed. 2006, 17, (1-2), 187-197.
- Yamaguchi, N.; Zhang, L.; Chae, B.-S.; Palla, C. S.; Furst, E. M.; Kiick, K. L., Growth
 Factor Mediated Assembly of Cell Receptor-Responsive Hydrogels. *J. Am. Chem. Soc.* 2007, 129, (11), 3040-3041.
- 24 44. Chien-Chi, L.; T., M. A., Metal-chelating affinity hydrogels for sustained protein release.
 25 J. Biomed. Mater. Res., Part A 2007, 83A, (4), 954-964.
- Luchini, A.; Geho, D. H.; Bishop, B.; Tran, D.; Xia, C.; Dufour, R. L.; Jones, C. D.;
 Espina, V.; Patanarut, A.; Zhou, W.; Ross, M. M.; Tessitore, A.; Petricoin, E. F.; Liotta,
 L. A., Smart Hydrogel Particles: Biomarker Harvesting: One-Step Affinity Purification,
 Size Exclusion, and Protection against Degradation. *Nano Lett.* 2008, 8, (1), 350-361.
- Vincent, H.; G., W. R., Competitive Affinity Release for Long-Term Delivery of Antibodies from Hydrogels. *Angew. Chem., Int. Ed.* **2018,** 57, (13), 3406-3410.
- 47. Lin, C.-C.; Anseth, K. S., Controlling Affinity Binding with Peptide-Functionalized Poly(ethylene glycol) Hydrogels. *Adv. Funct. Mater.* **2009**, 19, (14), 2325-2331.
- 34 48. Branco, M. C.; Pochan, D. J.; Wagner, N. J.; Schneider, J. P., Macromolecular diffusion
 35 and release from self-assembled β-hairpin peptide hydrogels. *Biomaterials* 2009, 30, (7),
 36 1339-1347.

- Lin, C.-C., Recent advances in crosslinking chemistry of biomimetic poly(ethylene glycol) hydrogels. *RSC Adv.* **2015**, 5, (50), 39844-39853.
- 50. Fisher, S. A.; Baker, A. E. G.; Shoichet, M. S., Designing Peptide and Protein Modified Hydrogels: Selecting the Optimal Conjugation Strategy. *J. Am. Chem. Soc.* **2017**, 139,
- 5 (22), 7416-7427.
- Vermonden, T.; Censi, R.; Hennink, W. E., Hydrogels for Protein Delivery. *Chem. Rev.* **2012**, 112, (5), 2853-2888.
- 8 52. Hilpert, K.; Hansen, G.; Wessner, H.; Küttner, G.; Welfle, K.; Seifert, M.; Höhne, W.,
- 9 Anti-c-myc antibody 9E10: epitope key positions and variability characterized using
- peptide spot synthesis on cellulose. *Protein Eng., Des. Sel.* **2001,** 14, (10), 803-806.
- 11 53. Hermanson, G. T., *Bioconjugate Techniques*. Elsevier Science: 2013.
- 12 54. Wang, R.; Johnson, J. A.; Olsen, B. D., Odd–Even Effect of Junction Functionality on the
- Topology and Elasticity of Polymer Networks. *Macromolecules* **2017**, 50, (6), 2556-
- 14 2564.
- 15 55. Mantid (2013): Manipulation and Analysis Toolkit for Instrument Data.
- 16 <u>http://dx.doi.org/10.5286/SOFTWARE/MANTID</u>
- Horkay, F.; Hammouda, B., Small-angle neutron scattering from typical synthetic and biopolymer solutions. *Colloid Polym. Sci.* **2008**, 286, (6), 611-620.
- 19 57. Hammouda, B.; Ho, D. L., Insight into chain dimensions in PEO/water solutions. J.
- 20 Polym. Sci., Part B: Polym. Phys. **2007**, 45, (16), 2196-2200.
- 21 58. Hammouda, B.; Ho, D. L.; Kline, S., Insight into Clustering in Poly(ethylene oxide)
- Solutions. *Macromolecules* **2004,** 37, (18), 6932-6937.
- 23 59. Vira, S.; Mekhedov, E.; Humphrey, G.; Blank, P. S., Fluorescent labeled antibodies -
- balancing functionality and degree of labeling. *Anal. Biochem.* **2010,** 402, (2), 146-150.
- 25 60. Seader, J. D.; Henley, E. J.; Roper, D. K., Separation Process Principles, 3rd Edition.
- John Wiley Incorporated: 2010.
- 27 61. Merrill, E. W.; Dennison, K. A.; Sung, C., Partitioning and diffusion of solutes in
- 28 hydrogels of poly(ethylene oxide). *Biomaterials* **1993**, 14, (15), 1117-1126.
- 29 62. Hill, T. L., An Introduction to Statistical Thermodynamics. Dover Publications: 2012.
- 30 63. de Gennes, P. G., Scaling Concepts in Polymer Physics. Cornell University Press: 1979.
- 31 64. de Gennes, P. G., Suspensions colloidales dans une solution de polymeres. C. R. Acad.
- 32 *Sci.* **1979**, 288, (21), 359-361.

- 1 65. Odijk, T., Protein–Macromolecule Interactions. *Macromolecules* **1996,** 29, (5), 1842-2 1843.
- 3 66. Wilkins, D. K.; Grimshaw, S. B.; Receveur, V.; Dobson, C. M.; Jones, J. A.; Smith, L. J.,
- 4 Hydrodynamic Radii of Native and Denatured Proteins Measured by Pulse Field Gradient
- 5 NMR Techniques. *Biochemistry* **1999**, 38, (50), 16424-16431.
- 67. Isgro, T. A.; Schulten, K., Association of Nuclear Pore FG-repeat Domains to NTF2 Import and Export Complexes. *J. Mol. Biol.* **2007**, 366, (1), 330-345.
- 8 68. Mian, I. S.; Bradwell, A. R.; Olson, A. J., Structure, function and properties of antibody binding sites. *J. Mol. Biol.* **1991**, 217, (1), 133-151.
- 10 69. Padlan, E. A., Anatomy of the antibody molecule. *Mol. Immunol.* **1994,** 31, (3), 169-217.
- 11 70. Merritt, E. A.; Hol, W. G. J., AB5 toxins. Curr. Opin. Struct. Biol. 1995, 5, (2), 165-171.
- 12 71. Fan, E.; Merritt, E. A.; Verlinde, C. L. M. J.; Hol, W. G. J., AB5 toxins: structures and inhibitor design. *Curr. Opin. Struct. Biol.* **2000**, 10, (6), 680-686.
- 14 72. Hough, L. E.; Dutta, K.; Sparks, S.; Temel, D. B.; Kamal, A.; Tetenbaum-Novatt, J.;
- Rout, M. P.; Cowburn, D., The molecular mechanism of nuclear transport revealed by
- atomic-scale measurements. *eLife* **2015**, 4, e10027.
- 17 73. Milles, S.; Mercadante, D.; Aramburu, Iker V.; Jensen, Malene R.; Banterle, N.; Koehler,
- 18 C.; Tyagi, S.; Clarke, J.; Shammas, Sarah L.; Blackledge, M.; Gräter, F.; Lemke,
- 19 Edward A., Plasticity of an Ultrafast Interaction between Nucleoporins and Nuclear
- 20 Transport Receptors. *Cell* **2015**, 163, (3), 734-745.
- 21 74. Denning, D. P.; Patel, S. S.; Uversky, V.; Fink, A. L.; Rexach, M., Disorder in the
- 22 nuclear pore complex: The FG repeat regions of nucleoporins are natively unfolded.
- 23 *Proc. Natl. Acad. Sci. U. S. A.* **2003,** 100, (5), 2450-2455.
- 24 75. Denning, D. P.; Uversky, V.; Patel, S. S.; Fink, A. L.; Rexach, M., The Saccharomyces
- cerevisiae Nucleoporin Nup2p Is a Natively Unfolded Protein. J. Biol. Chem. 2002, 277,
- 26 (36), 33447-33455.
- 27 76. Phelps, E. A.; Enemchukwu, N. O.; Fiore, V. F.; Sy, J. C.; Murthy, N.; Sulchek, T. A.;
- Barker, T. H.; García, A. J., Maleimide Cross-Linked Bioactive PEG Hydrogel Exhibits
- 29 Improved Reaction Kinetics and Cross-Linking for Cell Encapsulation and In Situ
- 30 Delivery. Adv. Mater. 2012, 24, (1), 64-70.
- 77. Van Der Bruggen, P.; Zhang, Y.; Chaux, P.; Stroobant, V.; Panichelli, C.; Schultz, E. S.;
- Chapiro, J.; Van den Eynde, B. J.; Brasseur, F.; Boon, T., Tumor-specific shared
- antigenic peptides recognized by human T cells. *Immunol. Rev.* **2002**, 188, (1), 51-64.
- 34 78. Novellino, L.; Castelli, C.; Parmiani, G., A listing of human tumor antigens recognized
- 35 by T cells: March 2004 update. *Cancer Immunol. Immunother.* **2005,** 54, (3), 187-207.

- 1 79. Dell, Z. E.; Schweizer, K. S., Theory of Localization and Activated Hopping of
- Nanoparticles in Cross-Linked Networks and Entangled Polymer Melts. *Macromolecules*
- **2014,** 47, (1), 405-414.
- 4 80. Cai, L.-H.; Panyukov, S.; Rubinstein, M., Hopping Diffusion of Nanoparticles in
- 5 Polymer Matrices. *Macromolecules* **2015**, 48, (3), 847-862.
- Parrish, E.; Caporizzo, M. A.; Composto, R. J., Network confinement and heterogeneity slows nanoparticle diffusion in polymer gels. *J. Chem. Phys.* **2017**, 146, (20), 203318.
- 8 82. Zhong, M.; Wang, R.; Kawamoto, K.; Olsen, B. D.; Johnson, J. A., Quantifying the
- 9 impact of molecular defects on polymer network elasticity. *Science* **2016**, 353, (6305),
- 10 1264-1268.
- 11 83. Zhou, H.; Woo, J.; Cok, A. M.; Wang, M.; Olsen, B. D.; Johnson, J. A., Counting
- 12 primary loops in polymer gels. *Proc. Natl. Acad. Sci. U. S. A.* **2012,** 109, (47), 19119-
- 13 19124.
- 14 84. Kawamoto, K.; Zhong, M.; Wang, R.; Olsen, B. D.; Johnson, J. A., Loops versus Branch
- Functionality in Model Click Hydrogels. *Macromolecules* **2015**, 48, (24), 8980-8988.
- 16 85. Wang, R.; Alexander-Katz, A.; Johnson, J. A.; Olsen, B. D., Universal Cyclic Topology
- in Polymer Networks. *Phys. Rev. Lett.* **2016**, 116, (18), 188302.
- 18 86. Wang, R.; Lin, T.-S.; Johnson, J. A.; Olsen, B. D., Kinetic Monte Carlo Simulation for
- 19 Quantification of the Gel Point of Polymer Networks. ACS Macro Lett. 2017, 6, (12),
- 20 1414-1419.
- 21 87. Lu, Q.; Solomon, M. J., Probe size effects on the microrheology of associating polymer
- solutions. *Phys. Rev. E* **2002**, 66, (6), 061504.
- 23 88. Cai, L.-H.; Panyukov, S.; Rubinstein, M., Mobility of Nonsticky Nanoparticles in
- 24 Polymer Liquids. *Macromolecules* **2011**, 44, (19), 7853-7863.
- 25 89. Armstrong, J. K.; Wenby, R. B.; Meiselman, H. J.; Fisher, T. C., The Hydrodynamic
- Radii of Macromolecules and Their Effect on Red Blood Cell Aggregation. *Biophys. J.*
- **2004,** 87, (6), 4259-4270.
- 28 90. Emilsson, G.; Schoch, R. L.; Feuz, L.; Höök, F.; Lim, R. Y. H.; Dahlin, A. B., Strongly
- 29 Stretched Protein Resistant Poly(ethylene glycol) Brushes Prepared by Grafting-To. ACS
- 30 *Appl. Mater. Interfaces* **2015,** 7, (14), 7505-7515.
- 31 91. Rapsomaniki, M. A.; Kotsantis, P.; Symeonidou, I.-E.; Giakoumakis, N.-N.; Taraviras,
- 32 S.; Lygerou, Z., easyFRAP: an interactive, easy-to-use tool for qualitative and
- quantitative analysis of FRAP data. *Bioinformatics* **2012**, 28, (13), 1800-1801.
- 34 92. Gao, H.; Wu, X.; Chai, J.; Han, Z., Crystal structure of a TALE protein reveals an
- extended N-terminal DNA binding region. *Cell Res.* **2012**, 22, 1716.

- Dahlke, K.; Sing, C. E., Facilitated Dissociation Kinetics of Dimeric Nucleoid-Associated Proteins Follow a Universal Curve. *Biophys. J.* **2017**, 112, (3), 543-551.
- 94. Dam, T. K.; Brewer, C. F., Effects of Clustered Epitopes in Multivalent Ligand-Receptor Interactions. *Biochemistry* **2008**, 47, (33), 8470-8476.

1 For Table of Contents Only

